Electr Eng (2012) 94:125–134
DOI 10.1007/s00202-011-0218-2

ORIGINAL PAPER

# An alternative approach to fault location on power distribution feeders with embedded remote-end power generation using artificial neural networks

**Yilmaz Aslan**

Received: 7 February 2008 / Accepted: 5 June 2011 / Published online: 13 September 2011


**Abstract** In this paper, the design and implementation of a feed-forward artificial neural network (ANN)-based fault locator to classify and locate shunt faults on primary overhead power distribution lines with load taps and embedded remote-end power generation is presented. In the ANN algorithm, the standard back-propagation technique with a sigmoid activation function is used. The fault locator utilizes fault voltage and current samples obtained at a single location of a typical radial distribution system. The ANNs are trained with data under a wide variety of fault conditions and used for the fault type classification and fault location on the distribution line. A 34.5 kV distribution system is simulated using electro-magnetic transients program and their results are used to train and test the ANNs. The ANN-based fault locator gives high accuracy for the vast majority of the practically encountered systems and fault conditions, including the presence of load taps and the remote-end in-feed source.

**Keywords** Fault location · Distribution lines · Artificial neural networks · Embedded generation

## 1 Introduction

In recent years, as a result of the competition with the privatisation of the power distribution companies, it has been become essential to provide the customers a high-quality service without any outages. Consequently, it is needed for these companies to locate permanent and transient faults on distribution feeders as quickly as possible. The importance of the fast fault locators is more obvious for the cases where foot patrols are relied upon, particularly, on relatively long lines and when the visibility is very poor because of tree growth, etc. Also, the locators can help in the case that maintenance is shared by many companies or divisions within a company. Moreover, the weak spots that are not obvious may be found and a more focused inspection can be performed within a limited area defined by the fault locator [1].

Although, so far, the majority of the distribution systems comprise feeders with remote ends open, due to the privatisation of the electricity supply industries and also increasing environmental and global concerns, more and more non-conventional energy sources such as wind energy, biogas, solar and small hydro, etc. are being added to the existing distribution systems. This trend is likely to continue in the near future [2]. An important problem due to increase in complexity of the distribution system arises from the fact that any fault will also have remote in-feed. It is well known that a remote-end in-feed can adversely affect the accuracy of the conventional fault locators. A number of the impedance-based fault location techniques for the single-ended overhead distribution systems have been proposed in [3–5]. In such techniques, the effects of pre-loading the presence of remote-end source and errors originating from the interface and the quantization are not taken into consideration. The technique developed in [6] is based on superimposing the components which is very efficient in distribution lines with remote-end generation, but it requires exact knowledge of the feeder configuration and the load data. A technique based on the travelling waves and high-frequency (HF) components presented in [7,8] requires specifically tuned filters, and its initial costs would be prohibitively high in longer radial distribution lines. In Refs. [9,10] the knowledge-based approaches which often require external information such as substation and feeder switch status, feeder measurements, load voltage and current sensors etc. are presented. The techniques devel-

Y. Aslan (✉)
Department of Electrical and Electronics Engineering, Faculty of Engineering, Dumlupinar University, 43100 Kutahya, Turkey
e-mail: yaslan@dumlupinar.edu.tr

oped in [11–16] require a dedicated communication medium. In addition, the recorded fault data gathered from the ends of the transmission system are needed to be synchronised. Although these techniques offer very accurate results, they are not tested for an overhead distribution system and also their initial investment and operational costs are too high. In Ref. [17], an intelligent two-port numerical algorithm for the fault location, the adaptive autoreclosure, the detailed disturbance record analysis and the fault data management is presented. The proposed algorithm does not require a synchronized sampling of the data taken from the line terminals and also the fault arc is included in the complete fault model. This algorithm, in contrast to the approaches that do not take the fault arc into consideration, gives a high accuracy in fault location and has the ability to determine both the arc and the fault/tower-footing resistance. But, the algorithm has not been tested for a practical low voltage overhead distribution feeder with load taps, yet.

This paper introduces a new approach based on ANNs to accurately locate shunt faults on primary overhead power distribution systems with load taps and also in the presence of small-scale distributed generation system connected at the remote-end of the network. The latter has a particular importance regarding the fact that the future distribution networks will increasingly become active (i.e. bi-directional power flow) due to the penetration of the renewable energy-based generation systems. Our technique is based on utilising the fault voltage and current samples obtained at a single location of a typical radial distribution line. In order to attain a high degree of accuracy in the location of a fault, the post-fault currents and voltages obtained from one end of the distribution system are filtered using Discrete Fourier Transform (DFT) techniques to extract the required power frequency components. The extracted voltage and current phasors are then fed to the ANN which has been trained off-line with the data under a wide variety of fault conditions to classify and locate the faults on the distribution line. The practical limitations originating from the hardware such as interface and quantization errors are taken into account in the design process. The proposed algorithm is practically tested in a 34.5 kV overhead distribution system through the simulations using the electro-magnetic transients program (EMTP). The accuracy of the technique is evaluated for the fault type, the location and the resistance, the presence of remote-end in-feed, the fault inception angle and the fault cycle. The simulation results clearly show that the proposed fault location technique presented here is highly accurate.

## 2 ANNs

Artificial neural networks are widely accepted and recognised method for the solution of the complex and ill-defined problems. Instead of using complicated mathematical methods and algorithms, ANNs can learn the key information from a multi-dimensional database. Moreover, since the ANNs can process the missing and noisy data, they have higher error tolerances. Another outstanding advantage of the ANN is that once trained they can produce fast results for nonlinear problems [18–20]. As seen in Fig. 1, the mathematical model of a basic ANN neuron has a much simpler structure comparing with a biological neuron. Basically, a neuron $k$ may be mathematically described with the Eqs. (1–3) [21]:

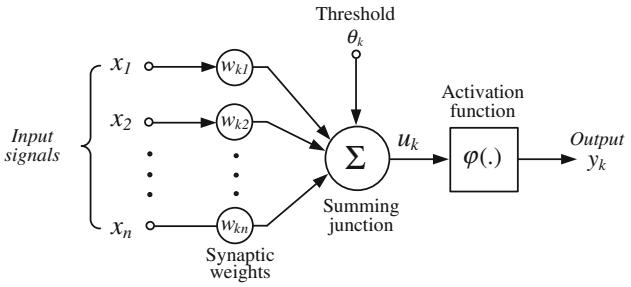


**Fig. 1** A basic structure of a neuron

$$u_k = \left( \sum_{i=1}^{n} w_{ki} x_i + \theta_k \right) \tag{1}$$

and

$$y_k = \varphi(u_k) \tag{2}$$

The data received from outer environment (or other neurons) $x_n$ are transferred to the neuron $k$ through weights $w_{kn}$ which adjust the effect of inputs. The neuron calculates a weighted average $(u_k)$ using the summation function and then uses some activation function $\varphi$ to produce an output $y_k$ [21]. The activation function is used to express the nonlinear relationship process between the input and the output data. The selection of the activation function may vary depending on the problem studied. In general, one of the activation functions of step, sign, sigmoid or linear is used. In this study, the log-sigmoid which is a nonlinear continuous function from 0 to 1 and differentiable everywhere for other $x$ values is preferred as an activation function. The mathematical expression of the log-sigmoid function is given in Eq. (3) [20]:

$$\varphi(x) = \frac{1}{1 + e^{-x}} \tag{3}$$

Figure 2 depicts the architecture of a typical feed-forward multilayered neural network which consists of an input layer, hidden layers (one or more) and an output layer. In the network, $x_n$ shows the inputs from outer environment to the first layer; $\overline{w}_{kn}$ and $w_{mk}$ are the weights applied to the second and the third layers, respectively. The number of the hidden layers and the number of neurons in the layers are subject to the problem studied and decided upon the trial-error.

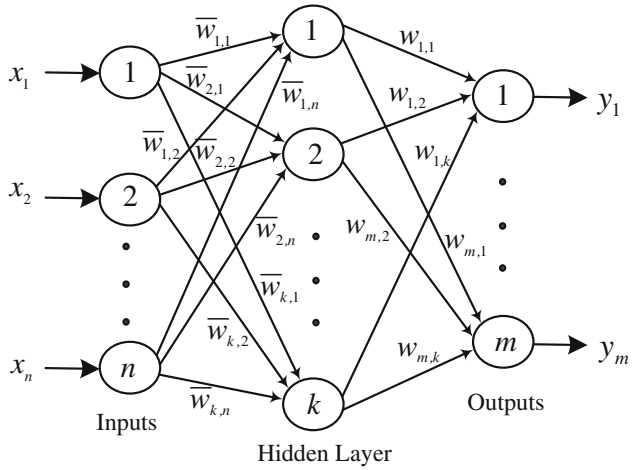


**Fig. 2** A feed-forward multi layer ANN

The input layer receives the signal from outer environment and distributes it to the neurons in the hidden layer. The number of hidden layers having computational neurons depends on the functions to be used. Since each additional layer increases the computing load exponentially, 3-layered ANNs are usually preferred in practice [18,19].

The training stages in the ANNs comprise both the feed-forward and back-propagation networks. After the training is completed, only the feed-forward algorithm is used in normal operation. Therefore, the training stage of the ANN is more time consuming when it is compared with the utilization stage.

## 3 ANN-based fault location algorithm

The complete fault locator scheme is shown in Fig. 3. The three-phase currents and voltages enter through the input transformers which provide a galvanic isolation from the instrument transformers as well as transforming the signals to ±10 V reference voltage level. The input signals taken from voltage transformers (VTs) and current transformers (CTs) may contain HF components under fault conditions. In order to prevent aliasing, second-order Butterworth filters with a cut-off frequency of 1.5 kHz are used. The filter outputs are switched in sequence by the multiplexer and fed into the sample and hold circuit in preparation for digital conversion. The analogue to digital conversion is achieved via a 12-bit A/D converter and a sampling frequency of 4 kHz (80 sample window) is used throughout the process. The $\pm 2^{11}$ conversion process leads to a quantisation level of approximately 4.8 mV. Analogue to digital conversion introduces further errors due to quantisation. After the digitisation stage, the voltage and current data is acquired and stored in a circular buffer in the RAM memory before being printed, processed or transmitted. The computer scans the voltage and the current samples, storing the data and the oldest information being overwritten.

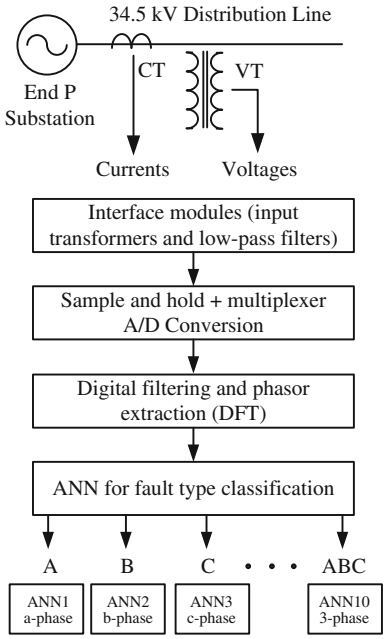


**Fig. 3** The complete fault location algorithm

### 3.1 Fault inception time identification

Before applying the fault location algorithm, any changes in stored current and voltage samples should be identified. In the digital fault recorder (DFR), after the digitisation stage, the microprocessor continuously executes a monitoring routine. In this process, the current and voltage samples taken from the near end of the distribution line are measured and stored in the RAM memory of the computer. In the presence of a fault, the current and the voltage waveforms are distorted and therefore, their magnitude and phase angle may change with respect to the pre-fault conditions. To identify the fault inception time, an adaptive approach is used and the first three samples of the second cycle are compared with the corresponding three samples of the previous cycle for the current waveform. Any significant change more than a predefined threshold level indicates the time at which the fault has occurred. If these criteria are not satisfied for the current samples, then the same process is applied to the voltage samples. Upon the inception of a fault, the fault recorder is triggered and the captured fundamental values of currents and voltages provide three cycles (or till the circuit breaker operates) of the fault data. In the development of the DFR, the important aspects of the practical fault recorders such as VT and CT responses, analogue interface effects and quantisation errors are taken into account. This is made to ensure that

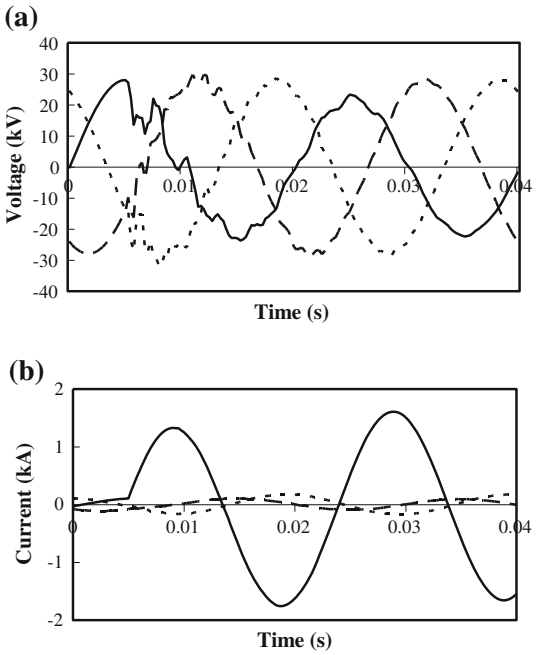


**Fig. 4** 'a'-phase-earth fault. **a** The three-phase voltages. **b** The three-phase currents

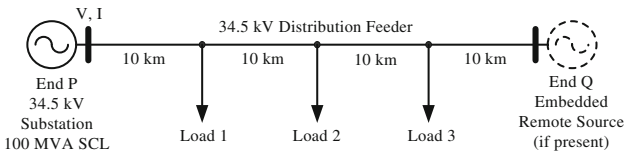


**Fig. 5** A 34.5 kV distribution system

the performance obtained is considerably close to a real-life situation.

### 3.2 The extraction of voltage and current phasors

Figure 4 shows the voltage and current waveforms for an 'a'-phase-earth fault at 3 km away from end $P$ in the system shown in Fig. 5. As can be seen in the waveforms, after the fault, the voltage waveforms are distorted due to HF components while DC off-set is more prominent in current waveforms.

In order to achieve a high degree of accuracy, in the fault location algorithm, after the A/D conversion it is vitally important to extract voltage and current phasors of the power frequency component from the post-fault waveforms which can contain transients ranging from high frequencies down to the DC levels. Although the Fast Fourier Transform (FFT) is superior to DFT in terms of computing performance, the computing time is relatively long since it calculates the entire frequency spectrum. In power protection systems, usually, only the power frequency (50 Hz) component is of interest. Since the DFT can be evaluated for any particular frequency component, it is more preferred in protection system applications [22]. The DFT is very efficient in rejecting the HF components and thus effectively attenuating the DC offset. It is applied to digitised voltage and current samples based on one cycle information which gives both the magnitude and the phase of the fundamental phasor $X_{v,i}(\omega)$ as [23,24]:

$$X_{v,i}(\omega) = \left(\frac{2}{N}\right) \sum_{n=0}^{n=N-1} \times \left[x_{v,i}(n)\left\{\cos(\omega n \Delta t) - j\ \sin(\omega n \Delta t)\right\}\right] \quad (4)$$

In Eq. (4), $N$ is the number of the samples per cycle, $\Delta t$ is the sampling time, $\omega$ is the frequency of the phasor to be extracted and $x_{v,i}(n)$ represents the sampled voltage or current waveforms. The phasors extracted from the DFT filter are used as the input to the fault type classifying ANN as shown in Fig. 3. When the classification of the fault type is achieved, to have a good generalization, the separate ANNs are used in accurately locating the types of the faults on the distribution system [25].

## 4 The practical considerations

As mentioned previously, the fault location technique in this work is based on utilising the voltage and the current phasors at the fault locator end of the line. Therefore, the training data is determined applying the following steps:

Step 1: The simulation of the distribution system with the EMTP to generate faulted voltage and current waveforms.
Step 2: The extraction of voltage and current phasors using a DFT filter.
Step 3: The application of the phasors to the designed best ANN topology.
Step 4: The calculation of the error between the output vector and the desired output and adjusting the weights to reduce the error.
Step 5: Repeating the process until the error criteria is satisfied.

In the testing stage, the weights are used to find the output values corresponding to the input values. In this stage, the errors are not propagated backward (from the output to the input) since it is not possible to compare the output data set with the target data set. A computer program written in Delphi is used to implement the ANN [26]. In the program, a three-layered ANN model with feed-forward and BP algorithms was used and some certain variables such as the learning rate, momentum and number of neurons in the layers can

**Table 1** The tested ANN parameters

| Neurons in the hidden layer | Number of iterations | Learning rate ($\eta$) | Momentum ($\alpha$) |
|---|---|---|---|
| | 10,000, 35,000, | 0.1 | 0.2 |
| $k$ | 50,000, 100,000 | 0.3 | 0.5 |
| | | 0.5 | 0.6 |

**Table 2** The output logic of the fault type classification ANN

| Fault type | $A$ | $B$ | $C$ | $G$ |
|---|---|---|---|---|
| No fault | 0 | 0 | 0 | 0 |
| 'a'-phase earth fault | 1 | 0 | 0 | 1 |
| 'a'-'b'-phase fault | 1 | 1 | 0 | 0 |
| 'a'-'b'-phase-earth fault | 1 | 1 | 0 | 1 |
| Three phase fault | 1 | 1 | 1 | 0 |

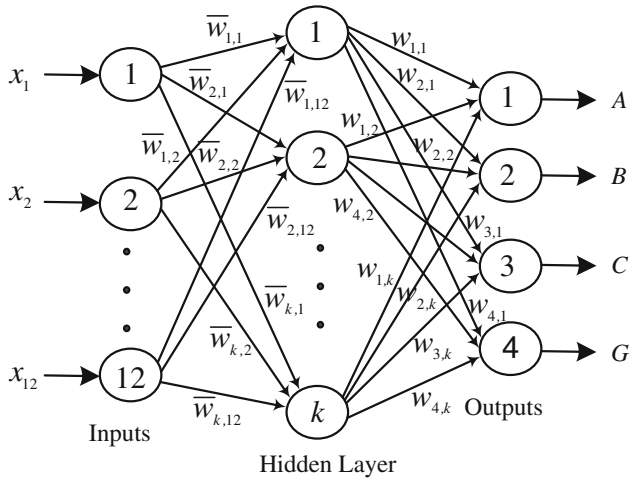


**Fig. 6** The ANN for the fault type classification

be changed. In the development stage of the ANN model, the proposed model has been tested using different parameters and number of iterations to find the best structure and to minimise the errors as shown in Table 1.

In the ANNs, although the estimation errors are reduced for a higher number of iterations, this results in a longer training time. In the development stage of the ANN model, it is seen after 35,000 iterations that the error is negligible and does not vary significantly. In this study, the number of neurons ($k$) in the hidden layer was varied as 8, 10, 12 and 14 neurons and the best results were achieved for 12 neurons in the hidden layer. Finally, a network with 12 neurons in the hidden layer and with log-sigmoid activation function was used. In the training stage, the learning rate ($\eta$) and the momentum ($\alpha$) were set to 0.5 and 0.6, respectively.

### 4.1 The simulation of a practical overhead power system

The practical distribution system studied in this work is a 34.5 kV, 50 Hz overhead system with three phase loads that each rated as 2 MVA with a power factor of 0.95 (lagging), tapped off at various locations as shown in Fig. 5. The overhead distribution lines employed in this work are aluminium–alloy conductors with no earth wires, based on horizontal line configuration currently used in the Turkish power distribution system. The overhead power distribution system is simulated with the EMTP software and the line elements are considered as distributed. The relevant data used are:

1. Earth resistivity (assumed homogeneous) = 100 Ωm.
2. Source $X/R$ ratio = 10; $Z_{s0}/Z_{s1} = 0.5$
3. 34.5 kV feeder impedance = $(0.18 + j0.34)$ Ω/km.

### 4.2 The training data for ANNs

In the development stage of an ANN-based algorithm, it is very important to train and test the network. The training data are obtained from the simulation of different types of faults at various points of a typical distribution system both with and without any remote-end source as shown in Fig. 5. The desired outputs of the ANN for fault type classification are defined by variables A, B, C and G. A value of unity for any of the first three variables corresponds to the 'a', 'b' or 'c' phases being faulty and a value of G near unity indicates that the ground is involved in a fault. Table 2 shows the output logic of the fault type classification ANN. In the developed algorithm, the voltage and current phasors are used as the training data representing the different fault and system conditions. The performance of the ANN was tested using the both patterns within and outside the training set. For a better accuracy and performance of the algorithm, the ANN was trained for the fault type classification; the separate networks are used for locating the faults on the distribution system. The desired output of the fault locating ANNs was defined as a specific point on the line in km [25]. Figure 6 shows the structure of the ANN for the fault type classification with four outputs and Fig. 7 shows one of the ANNs for the fault location which has one output. After the training, the networks were tested with a separate set of test data unseen by the ANNs before.

## 5 Results

The effectiveness of the developed technique was tested for different fault locations and types, fault resistance, fault inception angle and fault cycle. In all of the results presented here, the percentage error relating to fault location is based on the following equation:

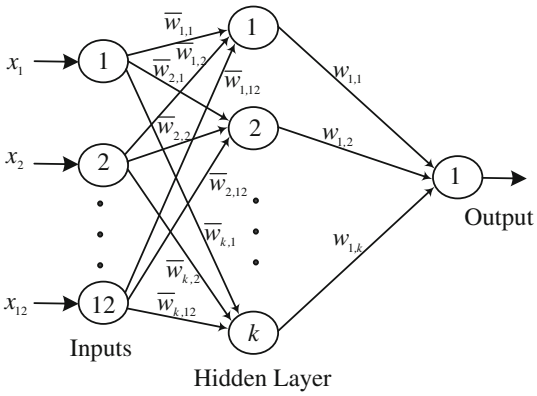


**Fig. 7** The ANN for the fault location

$$\text{error}\ (\%) = \frac{\text{actual location} - \text{desired location}}{\text{length of the line}} \times 100 \quad (5)$$

In order to show the effectiveness of the proposed technique, the training and the test data were generated using the 34.5 kV distribution system shown in Fig. 5. At every 2.5 km, the various faults were created and 80% of these cases were used for the training of the network and 20% were used for the subsequent testing. Table 3 shows the test results for the fault type classification. It is evident from the results that the ANN can accurately classify faults by giving the values around '1' and '2' since, in practice, the fluctuations are always exist [25].

### 5.1 The effects of the fault type and the location

Table 4 also classifies the effect of fault type for the faults in a 34.5 kV system shown in Fig. 5. The types of faults investigated are (AG) 'a'-phase-earth fault, (BG) 'b'-phase-earth fault, (CG) 'c'-phase-earth fault, (AB) 'a'-'b'-phases fault, (ABG) 'a'-'b'-phases-earth fault, (ABCG) 'a'-'b'-'c'-phases-earth fault. From the results, an increase in the error due to the phase-earth faults occurring near any tapping point can be observed. In these faulty conditions, the algorithm has yielded to a maximum error smaller than 3% for phase-earth faults created at 30 km on the system operated as radial (with no embedded source). These errors may be explained by the presence of laterals which lead to different fault currents for the faults occurring at different locations of a radial distribution feeder. It is evident from the results shown in Table 4 that the performance of the fault location algorithm, compared with the radial feeder, is not affected by the presence of the remote-end source.

The algorithm is also tested for the faults closer to the line ends. Various faults were created at 2.5 and 37.5 km on the radial operating system and with the 10 MVA source connected to the end of the system and the results are shown in Table 4. As can be seen, the results have not been significantly affected from the location and therefore the error has remained as less than 2% for all of the faults studied.

### 5.2 The effect of the fault resistance

The ANN was trained for the phase-earth faults for the fault resistance of 2, 5, 10, 15, 20, 30, 40, 50, 60, 80 and 100 Ω in the system shown in Fig. 5. The effect of the fault resistance on accuracy was tested on the same distribution system for the unseen cases and the results are given in Table 5. As seen from the table, the fault locator gives satisfactory results in the presence of fault resistance for the faults created at various locations. From the results it is observed that in contrast to the analytical methods the proposed method does not suffer from a high value of fault resistance ($R_f$). The algorithm was also tested for various fault resistances for an 'a'-phase-earth fault created at 30 km for the radial system (no remote-end in-feed) and the results are given in Fig. 8. As seen from the results, although the accuracy is varied with different fault resistances it had a variation of less than 3 % for the fault resistances studied.

In the overhead power distribution lines, the presence of the fault arc resistance which is a nonlinear phenomenon introduces HF transients particularly in the voltage waveforms during the shunt faults. In essence, these enhance the magnitudes of the transients present due to travelling waves. Since the proposed technique is based on the extraction of

**Table 3** The results of the fault classification

| Fault type | Desired output | | | | Actual output | | | |
|---|---|---|---|---|---|---|---|---|
| | *A* | *B* | *C* | *G* | *A* | *B* | *C* | *G* |
| AG | 1 | 0 | 0 | 1 | 1.008658 | −0.00597 | −0.00347 | 0.997666 |
| BG | 0 | 1 | 0 | 1 | −0.00049 | 0.997298 | 0.001566 | 1.008502 |
| CG | 0 | 0 | 1 | 1 | 0.005824 | −0.00332 | 1.00085 | 1.000501 |
| AB | 1 | 1 | 0 | 0 | 1.001126 | 0.994477 | 0.004847 | −0.00224 |
| ABG | 1 | 1 | 0 | 1 | 1.001272 | 0.99184 | −0.00062 | 1.000538 |
| ABCG | 1 | 1 | 1 | 1 | 1.004145 | 0.932686 | 1.010033 | 1.055676 |

**Table 4** The effect of the fault type and the location

| Fault type | Remote source capacity (MVA) | Fault resistance (Ω) | Fault location (km) | | Error (%) |
|---|---|---|---|---|---|
| | | | Desired output | Actual output | |
| AG | 0 | 2 | 2.5 | 2.418 | −0.21 |
| AG | 0 | 50 | 2.5 | 2.651 | 0.38 |
| AG | 0 | 100 | 2.5 | 2.787 | 0.72 |
| AG | 0 | 2 | 12.5 | 12.480 | −0.05 |
| AG | 0 | 50 | 12.5 | 12.445 | −0.14 |
| AG | 0 | 100 | 12.5 | 12.202 | −0.75 |
| AG | 0 | 2 | 30.0 | 29.348 | −1.63 |
| AG | 0 | 50 | 30.0 | 29.477 | −1.30 |
| AG | 0 | 100 | 30.0 | 28.822 | −2.95 |
| AG | 0 | 2 | 37.5 | 37.188 | −0.78 |
| AG | 0 | 50 | 37.5 | 36.992 | −1.27 |
| AG | 0 | 100 | 37.5 | 36.887 | −1.53 |
| BG | 0 | 2 | 12.5 | 12.274 | −0.57 |
| BG | 0 | 50 | 12.5 | 11.967 | −1.33 |
| BG | 0 | 100 | 12.5 | 12.141 | −0.90 |
| BG | 0 | 2 | 30.0 | 29.602 | −1.00 |
| BG | 0 | 50 | 30.0 | 29.058 | −2.36 |
| BG | 0 | 100 | 30.0 | 30.141 | 0.35 |
| CG | 0 | 2 | 12.5 | 12.690 | 0.48 |
| CG | 0 | 50 | 12.5 | 13.067 | 1.42 |
| CG | 0 | 100 | 12.5 | 12.638 | 0.35 |
| CG | 0 | 2 | 30.0 | 29.432 | −1.43 |
| CG | 0 | 50 | 30.0 | 29.874 | −0.32 |
| CG | 0 | 100 | 30.0 | 30.328 | 0.82 |
| AG | 10 | 2 | 12.5 | 12.493 | −0.02 |
| AG | 10 | 50 | 12.5 | 12.445 | −0.14 |
| AG | 10 | 100 | 12.5 | 12.664 | 0.41 |
| AG | 10 | 2 | 30.0 | 29.779 | −0.56 |
| AG | 10 | 50 | 30.0 | 29.929 | −0.18 |
| AG | 10 | 100 | 30.0 | 29.995 | −0.01 |
| AB | 0 | 0 | 2.5 | 2.619 | 0.30 |
| AB | 0 | 0 | 12.5 | 12.542 | 0.11 |
| AB | 0 | 0 | 30.0 | 29.998 | −0.01 |
| AB | 0 | 0 | 37.5 | 37.289 | −0.53 |
| AB | 10 | 0 | 2.5 | 3.370 | −0.33 |
| AB | 10 | 0 | 12.5 | 12.520 | 0.05 |
| AB | 10 | 0 | 30.0 | 30.004 | 0.01 |
| AB | 10 | 0 | 37.5 | 37.883 | 0.96 |
| ABG | 0 | 0 | 2.5 | 2.412 | −0.22 |
| ABG | 0 | 0 | 12.5 | 12.486 | −0.04 |
| ABG | 0 | 0 | 30.0 | 29.961 | −0.10 |
| ABG | 0 | 0 | 37.5 | 37.249 | −0.63 |
| ABG | 10 | 0 | 12.5 | 12.502 | 0.01 |
| ABG | 10 | 0 | 30.0 | 29.970 | −0.08 |
| ABCG | 0 | 0 | 12.5 | 12.482 | −0.01 |

**Table 5** The effect of the fault resistance

| Fault type | Source capacity (MVA) | | Fault resistance (Ω) | Fault location (km) | | Error (%) |
|---|---|---|---|---|---|---|
| | End P | End Q | | Desired output | Actual output | |
| AG | 100 | 0 | 2 | 22.5 | 22.607 | 0.27 |
| AG | 100 | 0 | 20 | 22.5 | 22.812 | 0.78 |
| AG | 100 | 0 | 50 | 22.5 | 22.178 | −0.81 |
| AG | 100 | 0 | 100 | 22.5 | 22.685 | 0.46 |
| AG | 100 | 10 | 2 | 22.5 | 22.587 | 0.22 |
| AG | 100 | 10 | 20 | 22.5 | 22.516 | 0.04 |
| AG | 100 | 10 | 50 | 22.5 | 22.523 | 0.06 |
| AG | 100 | 10 | 100 | 22.5 | 22.408 | −0.23 |

the power frequency phasors from the voltage and current waveforms, the transients present due to fault arc will only have little secondary effects on the accuracy. Of course, if the proposed technique is to be based on the transient components, then the integration of the accurate models for the fault arcs into the system model will be critical. In this work, only the linear arc resistances were considered. But importantly, of higher values as the latter has a significant influence on the magnitude of the power frequency components.

### 5.3 The effect of the fault inception time

In practice, the faults can occur at any point in the wave, i.e. the fault inception angle cannot be defined in advance. It is thus important to ascertain the algorithm's performance for the faults at inception angles rather than those near the maximum voltage. The tests were performed on the distribution system shown in Fig. 5 for the different inception angles of phase-earth faults and the results are summarised in Table 6. It is clearly evident from the results that the algorithm maintains a high degree of accuracy which is virtually independent of the fault inception angle.

### 5.4 The effect of the fault cycle

In the fault location algorithm, the DFT technique ignores the first cycle of post-fault data since the transients are most prominent during this period. However, there can be situations particularly under high-speed fault clearance that only the first cycle of information is available related to the fault location so it is no longer possible to ignore it. In these cases, all the post-fault information must be taken into account and it is thus important to ascertain the effect on the performance of the algorithm. A comparison of accuracy attained between utilising the first and second cycle of the data following an 'a'-phase-earth-fault on the distribution system is shown in Fig. 5 (no remote-end in-feed) and the results are summarised in Table 7. The results clearly show that the accuracy

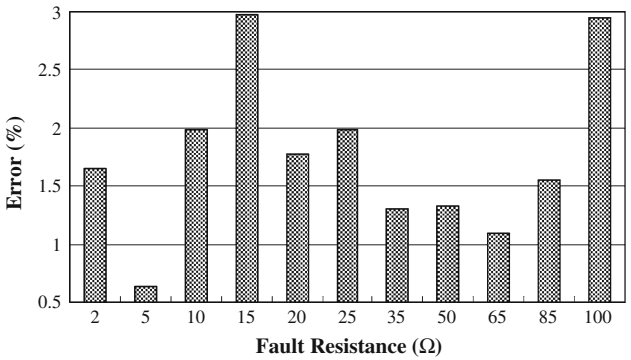


**Fig. 8** The effect of the fault resistance

is slightly affected for the defined faults using two cycles. But, in the case of the faults supplied with the data with a length of only one cycle, the accuracy is significantly affected for 'a'-phase-earth-faults created at 12.5 and 25 km with the estimation errors of 3.16 and 4.86%, respectively.

## 6 Conclusion

In this paper, an ANN-based fault location algorithm to classify and locate shunt faults on overhead power distribution feeders was presented. Our algorithm is based on utilising the fault voltage and current samples obtained at a single location of a typical radial distribution system with load taps and remote-end source. The main advantage of the algorithm over the other known fault location techniques is that there is no requirement for communication from the remote-end source and the exact knowledge of pre-fault loading. The proposed algorithm is less affected by the fault resistance, the fault type, the fault location and the embedded remote-end source, and the errors attained being less than 3 % for the majority of system and fault conditions studied here. Although the algorithm has been tested using CAD simulations, the practical

**Table 6** The effect of the fault inception angle

| Fault type | Remote source capacity (MVA) | Fault resistance (Ω) | Fault angle (°) | Fault location (km) | | Error (%) |
|---|---|---|---|---|---|---|
| | | | | Desired output | Actual output | |
| AG | 0 | 2 | 90 | 25.0 | 25.031 | 0.78 |
| AG | 0 | 2 | 135 | 25.0 | 24.977 | −0.08 |
| AG | 0 | 2 | 180 | 25.0 | 25.386 | 0.97 |
| AG | 0 | 2 | 225 | 25.0 | 25.089 | 0.23 |
| AG | 0 | 2 | 270 | 25.0 | 24.537 | −1.16 |

**Table 7** The effect of the fault cycle

| Fault type | Fault resistance (Ω) | Number of cycles used | Fault location (km) | | Error (%) |
|---|---|---|---|---|---|
| | | | Desired output | Actual output | |
| AG | 2 | 3 | 25.0 | 25.031 | 0.08 |
| AG | 2 | 2 | 25.0 | 25.041 | 0.10 |
| AG | 2 | 2 | 12.5 | 12.582 | 0.20 |
| AG | 2 | 1 | 12.5 | 13.762 | 3.16 |
| AG | 2 | 1 | 25.0 | 26.942 | 4.86 |

limitations of the hardware such as interface and quantization errors are taken into account in the design process.

The results show that the overall performance of the algorithm is significantly better compared with to the conventional techniques, particularly those based on impedance to fault measurements which give unacceptably high errors in the presence of the remote-end embedded generation and load taps. Although the algorithm was developed for the overhead power distribution systems, it can be applied to the composite systems consist of overhead lines and underground cable sections. Another major advantage of the algorithm is that the ANNs can be trained off-line with the data reflecting modifications on the existing system such as demographic data of the area and seasonal or daily energy demand and generation levels. Once the training is over, on-line fast and accurate fault clearance and diagnosis can be achieved in the distribution system with embedded electric power generation.

## References


1. Eriksson L, Saha MM, Rockefeller GD (1985) An accurate fault locator with compensation for apparent reactance in the fault resistance resulting from remote-end infeed. IEEE Trans Power Apparatus Syst 104(2):424–436
2. Singh GK (2004) Self-excited induction generator research—a survey. Electr Power Syst Res 69:107–114
3. Girgis AA, Fallon CM, Lubkeman DL (1993) A fault location technique for rural distribution feeders. IEEE Trans Ind Appl 29(6):1170–1175
4. Sachdev MS, Das R, Sidhu TS (1997) Determining locations of faults in distribution systems. In: Developments in power systems protection, 25–27th March 1997 Conference publication no: 434, IEE, pp 188–191
5. Zhu J, Lubkeman DL, Girgis AA (1996) Automated fault location and diagnosis on electric power distribution feeders. IEEE Winter Meet 12:1–8
6. Aggarwal RK, Aslan Y, Johns AT (1997) A new concept in fault location for overhead distribution systems using superimposed components. IEE Proc Gener Transm Distrib 144(3):309–316
7. El-Hami M, Lai LL, Daruvvala DJ, Johns AT (1994) A new travelling-wave based scheme for fault detection on overhead power distribution feeders. IEEE Trans Power Deliv 17(4):1825–1833
8. Johns AT, Lai LL, El-Hami M, Daruvvala DJ (1991) A new approach to directional fault locator for overhead power distribution feeders. IEE Proc Gener Transm Distrib 138(2):351–357
9. Jarventausta P, Verho P, Partanen J. (1994) Using fuzzy sets to model the uncertainty in the fault location process of distribution networks. IEEE Trans Power Deliv 9(2):954–960
10. Hsu YY, Lu FC, Chien Y, Liu JP, Lin JT, Yu HS, Kuo RT (1991) An expert system for locating distribution system faults. IEEE Trans Power Deliv 6(1):336–372
11. Kezunovic M, Perunicic B, Mrkie J (1994) An accurate fault location algorithm using synchronised sampling. Electr Power Syst Res 29(3):161–169
12. Luo S, Kezunovic M, Sevick DR (2004) Locating faults in the transmission network using sparse field measurements, simulation data and genetic algorithm. Electr Power Syst Res 71:169–177
13. Gopalakrishnan A, Kezunovic M, Mckenna SM, Hamai DM (2000) Fault location using the distributed parameter transmission line model. IEEE Trans Power Deliv 15(4):1169–1172
14. Kezunovic M, Perunicic B (1996) Automated transmission line fault analysis using synchronised sampling at two ends. IEEE Trans Power Syst 11(1):441–447
15. Radojević Z, Terzija VV (2007) Effective two-terminal algorithm for overhead lines protection. Electr Eng (Archiv für Elektrotechnik), 89:425–432

16. Radojević Z, Terzija VV (2006) Two terminals numerical algorithm for fault distance calculation and fault analysis. In: Power systems conference and exposition, 29th October–1st November 2006, IEEE PES, pp 1037–1042
17. Radojević Z, Terzija VV (2008) Intelligent two-port numerical algorithm for transmission lines disturbance record analysis. Electr Eng (Archiv für Elektrotechnik) 90:323–330
18. Beccali M, Cellura M, Lo Brano V, Marvuglia A (2004) Forecasting daily urban electric load profiles using artificial neural networks. Energy Convers Manag 45:2879–2900
19. Kalogirou SA (1999) Applications of artificial neural networks in energy systems: a review. Energy Convers Manag 40:1073–1087
20. Ilunga M, Stephenson D (2005) Infilling stream flow data using feed-forward back-propagation (BP) artificial neural networks: Application of standard BP and pseudo Mac Laurin power series BP techniques. Water SA 31(2):171–176
21. Haykin S (1994) Neural networks, a comprehensive foundation. Prentice-Hall, New Jersey
22. Moore PJ (1997) Power system protection. Digital protection and signalling. The Institution of Electrical Engineers, UK, vol 4, pp 32–36
23. Gu JC, Yu S (2000) Removal of dc offset in current and voltage signals using a novel filter algorithm. IEEE Trans Power Deliv 15(1):73–79
24. Purushothama GK, Narendranath AU, Thukaram D, Parthasarathy K (2001) ANN applications in fault locators. Electr Power Energy Syst 23:491–506
25. Joorabian M, Taleghani Asl SMA, Aggarwal RK (2004) Accurate fault locator for EHV transmission lines based on radial basis function neural networks. Electr Power Syst Res 71:195–202
26. Temurtas H (2004) The joint based trajectory control with neural generalized predictive control for a three joint robotic manipulator PhD. thesis, Sakarya University, Turkey